MATHEMATICAL BIOSCIENCES
AND ENGINEERING
Volume **10**, Number **3**, June **2013**

doi:10.3934/mbe.2013.10.939

pp. **939–957**

COMPUTATIONAL MODELING APPROACHES TO STUDYING THE DYNAMICS OF ONCOLYTIC VIRUSES

Dominik Wodarz

Department of Ecology and Evolutionary Biology
University of California
321 Steinhaus Hall, Irvine, CA 92617, USA

Abstract. Oncolytic viruses specifically infect cancer cells, replicate in them, kill them, and spread to further tumor cells. They represent a targeted treatment approach that is promising in principle, but consistent success has yet to be observed. Mathematical models can play an important role in analyzing the dynamics between oncolytic viruses and a growing tumor cell population, providing insights that can be useful for the further development of this therapy approach. This article reviews different mathematical modeling approaches ranging from ordinary differential equations to spatially explicit agent-based models. Problems of model robustness are discussed and so are some clinically important insight derived from the models.

1. **Introduction.** Oncolytic viruses replicate selectively in tumor cells and have been explored as a targeted treatment approach against cancers [1-15]. In principle an oncolytic virus will spread though the tumor cell population and lyse the infected cells, leading to eradication or control of the tumor. Because of the selectivity of such viruses for cancer cells rather than normal human cells, side effects also should be less pronounced than those associated with traditional treatments, such as chemotherapy or ionizing radiation. Oncolytic virus therapy has been explored in the context of several different virus species. While some non-human viruses display natural selectivity for cancer cells in humans [16], modern approaches use genetically engineered viruses to achieve tumor selectivity. The first engineered virus generated in the 1990s was a herpes simplex virus-1 [17]. Engineered adenoviruses have been of major interest in recent clinical trials, especially in the context of head and neck cancer [15]. Indeed the adenovirus H101(Shanghai Sunway Biotech, Shanghai, China) was approved in China for the treatment of head and neck cancer in combination with chemotherapy [18]. A variety of other virus types has also been explored [19]. However despite initial promising results and observations in the laboratory and clinic, oncolytic viruses have so far failed to demonstrate sustained and reliable treatment success [15].

Besides experimental research, mathematical and computational modeling has increasingly become a tool to study the dynamics of oncolytic viruses. Mathematical models can help us understand the emerging properties of cancer-virus interactions,

2010 *Mathematics Subject Classification.* 92D25.

Key words and phrases. Oncolytic viruses, cancer, therapy, mathematical models, population dynamics, spatial dynamics.

This work was funded in part by NIH grant 1R01AI093998-01A1.

to interpret experimental results, and to design new experiments. The first mathematical models of oncolytic virus therapy considered ordinary differential equations that described the basic interactions between a replicating virus and a growing population of tumor cells, and also immune responses [20, 21]. Further work extended this type of approach in a number of ways, describing different scenarios and applying models to specific virus-tumor systems [22-35]. One of the assumptions that is implicit in such modeling approaches is that cells and viruses mix perfectly with each other (mass action). While this might hold true in the context of some in vitro experiments, and while this might be a reasonable approximation of the dynamics occurring in some non-solid tumors, the majority of tumors have intricate spatial structures where cells and viruses do not mix well, but where interactions are limited to local neighborhoods. Hence, to gain a better understanding about the dynamics of oncolytic viruses, spatially explicit models are required. Some spatial modeling studies have been performed and have given rise to interesting results [30, 36-38]. They commonly include, in addition to basic spatial dynamics, one or more additional assumptions that introduce further complexity.

This review summarizes our own modeling approaches to studying the dynamics of oncolytic viruses. The aim is to highlight the usefulness and limitations of different modeling approaches in the quest to obtain an accurate model that can be applied to specific treatments and provide predictive power. The article starts by discussing specific ordinary differential equation (ODE) models, continues to describe more general, axiomatic modeling approaches, and finally examines a spatially explicit model describing virus dynamics in relatively simple in vitro settings.

2. **A basic ordinary differential equation model.** This section introduces a simple mathematical model describing the development of a growing tumor and an oncolytic virus population over time. The model is based on [20] and includes three variables: the growing , uninfected, cancer cells, x, infected cancer cells, y, and virus particles, v. It is given by the following set of differential equations which describe the development of these populations over time [31]:

$$\begin{aligned} \frac{dx}{dt} &= rx\left(1-\frac{x+y}{\omega}\right) - dx - \beta xv \\ \frac{dy}{dt} &= \beta xv - (d+a)y \\ \frac{dv}{dt} &= ky - uv \end{aligned} \tag{1}$$

The cancer cells grow at a rate rx, and this growth is density dependent, limited by a maximum size ω. In biological terms, this means that the cancer cells divide and that this results in exponential growth at small tumor cell densities, but that growth is slowed down as the tumor reaches larger sizes and runs out of space, nutrients, and other resources required for growth. Cancer cells die at a rate dx. Therefore, the average life-span of the cancer cells is given by $1/d$. The cancer cells become infected by the virus at a rate βxv. The rate constant, β, describes the efficacy of this process, including the rate at which virus particles find uninfected cells, the rate of virus entry, and the rate of successful infection. The term βxv multiplied by a time interval gives the number of infection events occurring during the time interval (if it is assumed to be small). Infected cancer cells also have a death rate. The death rate of infected cells is a composite of the natural death rate, dy, and the virus-inflicted death rate, ay. Therefore, the average life-time of

an infected cell is $1/(d+a)$. Infected cells produce virus at a rate ky. The total amount of virus particles produced from one infected cell , or the "burst size", is hence given by $k/(a+d)$. Finally, the virus decays at a rate uv. Thus, the average life-span of a virus particle is given by $1/u$. In the context of replicating versus non-replicating viruses, we can make the following distinction. A non-replicating virus is characterized by $k = 0$ (no virus production by the infected cell), while a replicating virus is characterized by $k > 0$.

In this model, the tumor expands if its growth rate is greater than its death rate, i.e. if $r > d$. In the absence of treatment, the tumor will eventually grow to its maximum size given by $x^{(0)} = \omega\ (r\text{-}d)\ /\ r$. Treatment in the model corresponds to the introduction of virus into the system. The virus has the potential to spread if $\beta x^{(0)} > d+a$, that is if the replication rate of the virus is fast relative to the death rate of the infected cancer cells. The virus infection then takes the system to a new equilibrium outcome which is given by the following expressions. $x^{(1)} = (d +$

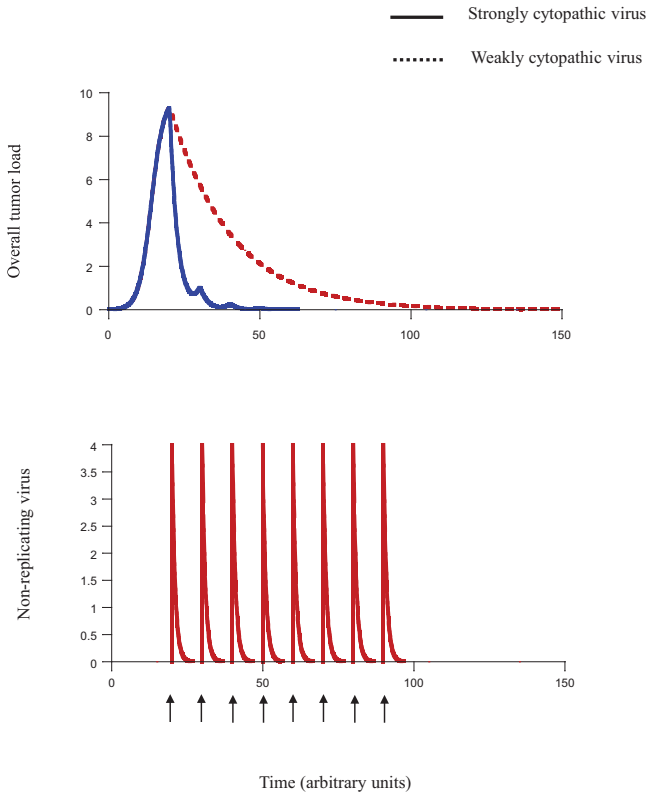

FIGURE 1. Simulation of therapy using a non-replicating virus. The virus is administered repeatedly, as indicated by the arrows. The development of tumor load over time is shown assuming both a strongly cytopathic virus and a weakly cytopathic virus. The strongly cytopathic virus results in more efficient eradication of the tumor. Parameters were chosen as follows. $r = 0.5$; $\omega = 10$; $\beta' = 1.5$; $d = 0.01$; $k = 0, \delta = 1$. For the strongly cytopahtic virus, $\alpha = 0.4$. For the weakly cytopathic virus, $\alpha = 0.04$.

$a)/\beta'; y^{(1)} = [\beta'\omega(r\text{-}d) - r(d+a)/[\beta'(r+\beta'\omega)]$; $v^{(1)} = ky^{(1)}/u$; where β' summarizes the overall replication rate of the virus and is given by $\beta' = \beta k/u$. The size of the overall tumor cell population during virus therapy is given by the sum of uninfected and infected tumor cells, $x^{(1)} + y^{(1)}$. The aim of therapy should be to reduce this population to low levels. If it has been reduced below a threshold in the model, the tumor population can be assumed to be extinct (number of tumor cells below one). In the following sections, model properties will be analyzed. Figures are shown to demonstrate specific aspects qualitatively, i.e. parameters were chosen for illustrative purposes and unites are arbitrary.

2.1. **Non-replicating viruses.** Assume the virus is not replicating ($k = 0$). If not all cancer cells become infected after the first administration, it has to be given repeatedly in order to ensure continued presence of the virus and hence remission of

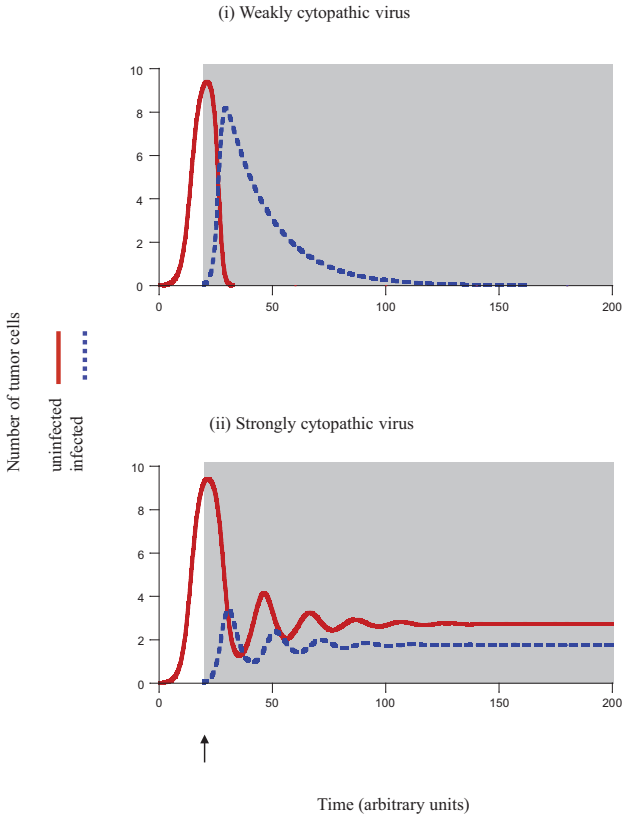

FIGURE 2. Simulation of therapy using a replicating virus. The virus is administered once, as indicated by the arrow. Shading indicates the phase of the dynamics following administration of the virus. (i) Use of a weakly cytopathic virus results in sustained cancer remission. (ii) Use of a more cytopathic virus results in long term persistence of the cancer and the virus. Parameters were chosen as follows: $r = 0.5$; $\omega = 10$; $\beta' = 1.5$; $d = 0.01$; $k = 0, 1$; $\delta = 1$. For (i) $\alpha = 0.04$. For (ii) $\alpha = 0.4$.

the cancer (Figure 1). The goal is to eradicate the population of uninfected tumor cells. Since infected cancer cells do not divide, they do not pose a threat and will decay to extinction. The dynamics of the uninfected cancer cell population over time during treatment can be approximated by $x_t = x^{(0)}\ exp[\ (t(r\text{-}d\text{-}\beta v)]$. This assumes that the tumor is still growing and has not yet reached levels close to maximum tumor size ($x << \omega$). For the uninfected cancer cells to decline, the level of virus has to be kept above a threshold during therapy, given by $v > (r\text{-}d)/\beta$. Thus, a high infectivity of the virus, and a low growth rate of the tumor facilitate tumor reduction. If this condition is fulfilled, the half-life of the uninfected tumor cell population is given by $t_{1/2} = ln(1/2)\ /\ (r - d - \beta v)$. The time to eradication of the uninfected tumor cells is hence given by $t = \frac{\ln(x_0)}{\ln(2)} \frac{\ln(1/2)}{r-d-\beta v}$. After this time threshold, administration of the virus can be stopped, and the population of infected tumor cells decays with a half-life of $t_{1/2} = ln(2)/a$. Hence, the faster the rate of virus-induced cell death, a, the faster the population of infected cells declines towards extinction (Figure 1). To summarize, the best strategy is to (i) use a cytopathic virus, (ii) use a virus with high infectivity, and (iii) reduce the cancer growth rate which might be achieved by certain chemo- or radio-therapeutic regimes [39].

2.2. **Replicating viruses.** Now assume a replicating virus (k >0). If the patient is injected with a very high inoculum dose of the virus, most or all cancer cells immediately become infected and the situation is the same as for the non-replicating virus. If, however, the initial virus inoculum is not that large and does not immediately overwhelm the cancer, then the dynamics between virus replication and tumor growth will play out, resulting in an equilibrium outcome. The size of the tumor load (infected + uninfected cells) at equilibrium determines the level of success. If equilibrium tumor load in the model is very low, this corresponds to eradication in practical terms. Higher equilibrium tumor loads in the model corresponds to persistence of the tumor in the presence of the virus. Equilibrium tumor load is given by $x^{(1)} + y^{(1)} = \frac{\omega(a+r)}{r+\beta'\omega}$. An important result is that a lower virus-induced death rate of infected cells (small a) results in lower equilibrium tumor load (Figure 2). If the rate of virus-induced tumor cell killing is too high, the outcome is persistence of the tumor in the face of ongoing viral replication (Figure 2). The reason is as follows. Low viral cytopathicity increases virus load. Higher virus load results in more infection and in a greater decline of the uninfected cancer cells. Higher viral cytopathicity results in lower virus load. Low virus load results in less infection and in less reduction of the uninfected tumor cells. In addition, equilibrium tumor load is reduced by other parameters, most notably by a high replication rate of the virus (high value of β'), and a slow growth rate of the tumor (low value of r). As expected, the replication rate of the virus (value of β') has to lie above a threshold for tumor load to become low enough that tumor eradication is feasible in a stochastic setting. If the replication rate of the virus is too low, the virus does not spread sufficiently through the population of tumor cells. In summary, if the virus is replicating, the best strategy is to (i) use a weakly cytopathic virus, (ii) use a fast replicating virus, and (iii) reduce the growth rate of the tumor by alternative therapeutic means.

2.2.1. *Evaluation of replicating viruses in culture.* The mathematical model has given rise to an important difference in treatment strategy depending on whether the virus replicates or not. If the virus does not replicate, a high degree of cytopathicity is beneficial because it speeds up elimination of all tumor cells. On the other hand,

if the virus replicates, success is promoted by using a weakly cytopathic virus. A high rate of virus-induced cell death is detrimental and leads to the persistence of both tumor and virus. These findings also have important implications for the methods used to evaluate potential viruses in culture. If the virus does not replicate, a high multiplicity of infection (MOI) has to be used. The virus with the strongest degree of tumor cell killing will remove the cancer cells fastest. Such a virus will also work best in the physiological situation, since the aim is to overwhelm the tumor by repeatedly injecting the agent, resulting in fast killing of as many cancer cells as possible (Figure 1). On the other hand, if the virus replicates, a low MOI is required to evaluate the virus. The reason is that *in vivo*, the replicating virus has to spread through the cancer cell population, and this has to be mimicked in culture. Using a high MOI can lead to misleading evaluations. These notions are illustrated in Figure 3 with computer simulations. This figure depicts the dynamics

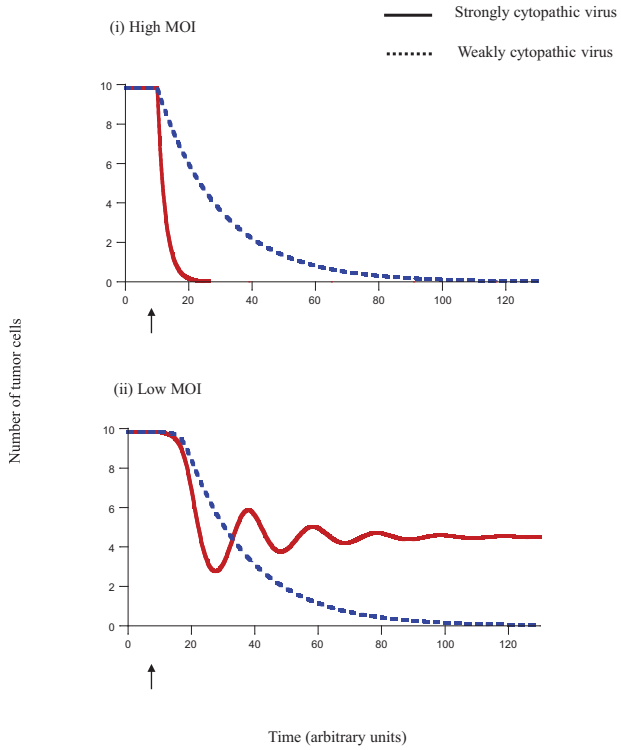

FIGURE 3. Simulation showing the evaluation of potential replicating viruses in culture. A weakly and a strongly cytopathic virus are compared when the culture is inoculated (see arrow) with (i) a high MOI and (ii) a low MOI. While under high MOI infection the more cytopathic virus yields better results, the opposite is true for low MOI infection, which reflects virus spread conditions in vivo. Parameters were chosen as follows. $r = 0.5$; $\omega = 10$; $\beta' = 1.5$; $d = 0.01$; $k = 0.1$; $\delta = 1$. For the strongly cytopahtic virus, $\alpha = 0.4$. For the weakly cytopathic virus, $\alpha = 0.04$. Virus inoculum was $v = 10$ for high MOI and $v = 0.01$ for low MOI.

in culture for strongly and weakly cytopathic viruses, using different MOIs. Figure 3i shows the dynamics for a high MOI. In this simulation, the strongly cytopathic virus results in quick elimination of the tumor cells, while the weakly cytopathic virus is much less effective. Thus, if viruses are evaluated using a high MOI, the virus with the strongest degree of tumor cell killing receives the highest grades. Importantly, this is the virus which is predicted to be least efficient at reducing tumor load *in vivo*. The situation is different when viruses are evaluated in culture using a low MOI (Figure 3ii). The less cytopathic virus results in elimination of tumor cells in culture, while the more cytopathic virus fails to eliminate tumor cells in culture. Therefore, the less cytopathic virus gets the better marks, and this is also the virus which is predicted to be more efficient at reducing tumor load *in vivo*.

3. **Different mathematical formulations and the robustness of results.** The above described model investigated the dynamics of oncolytic viruses in the context of specific mathematical formulations that are of uncertain biological nature. For example, consider the term that describes the infection of cells, given by βxv. It assumes perfect mixing of cells and viruses, which is hardly realistic in vivo, where most tumors exhibit intricate spatial structures. The larger the number of tumor cells, the faster the growth rate of the virus population. Similarly, the larger the number of viruses available, the more cells become infected, ignoring possible saturation effects. The "biologically correct" term to describe infection is currently not known. Other processes assumed in the model are also described by arbitrary mathematical expressions, such as the term describing cell growth, given by the logistic equation. While this is assumed in many models of tumor growth, the laws underlying tumor growth are likely to be more complex, and this could impact the properties of the virus dynamics model. To address this issue, we avoided concentrating on a particular model, but took a more general approach. Processes such as infection and cell growth were formulated in terms of general functions and results were thus independent from biologically uncertain and arbitrary mathematical formulations [33]. Through specific restrictions about biological assumptions, we analyzed a class of mathematical models that aim to describe viral spread through a tumor in different settings. Details of the mathematical analysis are given in [28].

We found that based on the infection term, we can divide models into two categories with fundamentally different behavior [33]. In one group, virus growth is relatively fast, which could be characteristic of a relatively well mixed system. In these models, there is a clear viral replication rate threshold beyond which the number of cancer cells drops to levels of the order of one or less, corresponding to extinction in practical terms. Under this parameter region, this is the only outcome in this class of model. In the other category, virus growth is relatively slow, which could be characteristic of more intricate tumor cell arrangements. In this class of model, the larger the number of infected cells, the smaller the proportion of cells that can pass on the virus. In this scenario, virus therapy is more difficult. If tumor growth saturates only at relatively large sizes or does not saturate, then even in the parameter regions where the dynamics can converge to a tumor control or eradication outcome, there can be the possibility that the cancer can outrun the virus if the number of cancer cells lies above a threshold at the start of virus therapy. This is because of the existence of the saddle node equilibrium which ensures dependence of the outcome on initial conditions. This might be problematic in clinical settings, because there is only a relatively small window between the size at which the tumor

becomes detectable (about 10^{10} cells) and the size at which it can induce mortality (around 10^{13} cells).Tumor growth saturation at lower levels introduces a parameter region in which only the tumor control outcome is possible. A further reduction in the number of tumor cells at which growth saturation occurs can abolish the existence of the saddle node equilibrium altogether. In this case, the only outcome is tumor control. This result makes intuitive sense: earlier saturation of tumor growth slows down the cancer, and makes it easier for the virus to gain the upper hand. It also means that if the tumor is found early, it might be possible to slow down tumor growth by means of more conventional drug therapy, enabling the virus to control the cancer and to prevent runaway growth. There is indication in clinical data that a combination of chemotherapy and oncolytic virus therapy leads to better results than either approach alone [40].

Another important finding of our study is that the basic results regarding the outcome of oncolytic virus therapy do not depend on the particular tumor growth terms used in the model [33]. The exact kinetics of tumor growth are still poorly understood and a source of uncertainty [41]. We examined straight exponential growth, as well as a number of more realistic options, including saturated but continued growth at high numbers of cancer cells, as well as cessation of growth as the number of tumor cells approaches an upper limit [28]. While there are minor differences, the properties of the tumor control equilibrium are largely independent from the exact way in which tumor growth is modeled.

4. **A spatially explicit model of oncolytic virus dynamics.** Tumors are characterized by intricate spatial structures that cannot be captured by ordinary differential equations. Other modeling methods have to be called upon in order to capture this complexity. On the other hand, the spatial complexity of tumors is enormous and not well understood, which can undermine the predictive power of such spatial models. As a first step to tackle this problem, we considered a relatively simple in vitro setting, in which target cells are arranged in a two-dimensional monolayer and in which viruses can only spread from the infected source cell to the nearest neighboring target cells [42]. This relatively simple experimental setting can be described by an agent-based model, and model predictions can be tested relatively easily by experiments. In the model, each cell is represented as an "agent" occupying a certain position on a grid, and interacting with other cells according to some (probabilistic) rules. Our modeling approach is spatial, that is, it takes into account the spatial distribution of the uninfected and infected cells. The model, based on [43], describes target cell-virus dynamics on a two dimensional grid that contains NxN spots [42]. Each spot is either occupied by a cell (infected or uninfected), or it is empty. We model the development of the populations in discrete time. Given the state of the system at time t, a set of rules is applied to each spot, and this gives rise to the state of the system at time $t+1$. At each time step, the grid is randomly sampled N^2 times. If the chosen spot is occupied by an uninfected cell, it can die with a probability D, leaving the spot empty. Alternatively, the cell can reproduce with a probability R, and a destination spot is randomly chosen for the offspring from the set of eight nearest neighboring spots . If the destination spot is empty, the offspring is placed there, otherwise, no reproduction occurs. If the chosen spot contains an infected cell, it can die with a probability A, or attempt to transmit the virus with a probability B. A destination spot is chosen randomly from the eight nearest neighbors, and infection only proceeds when a susceptible cell is present.

Infected cells are assumed not to reproduce. Typical oncolytic viruses lock the cell in the S-phase for replication, thus preventing further divisions [34].

4.1. **Initial virus growth patterns.** In this section, we explore the initial virus growth patterns. As starting conditions we assume that the grid is filled with uninfected cells and that a relatively small square of infected cells (30x30 spots) is placed in the middle of the grid (which overall contains 300x300 spots). The emerging growth pattern depends on parameters that influence the rate of virus spread, in particular the probability for an infected cell to die, A, and the probability for an infected cell to transmit the virus, B. The patterns that we observe are presented in Figure 4.

In Figures 4a and b, the infected cell population expands as a ring or wave that leaves no cell behind in its core. The two pictures differ in the death probability of infected cells. In Figure 4a, the probability for infected cells to die is relatively low

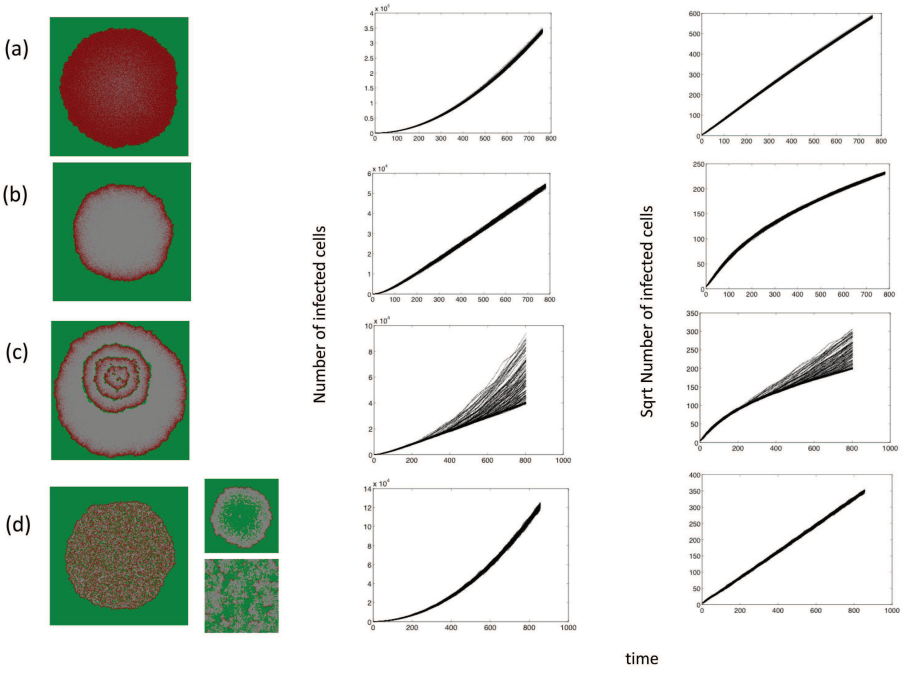

FIGURE 4. Initial virus growth dynamics in the agent-based model. Green indicates uninfected cells, red infected cells, and grey empty spots. The middle graph shows the number of infected cells over time. The different lines represents 100 different instances of the simulation with the same parameter combination. The right graph shows the square root of the number of infected cells over time, again showing lines for 100 different runs. Parameter values were chosen as follows. (a) $R = 0.5$; $D = 0$; $B = 0.6$; $A = 0.601$. (b) $R = 0.5$; $D = 0$; $B = 0.6$; $A = 0.62$. (c) $R = 0.5$; $D = 0$; $B = 0.6$; $A = 0.628$. (d) $R = 0.5$; $D = 0$; $B = 0.6$; $A = 0.7$. The small graphs in (d) are characterized by $R = 0.04$, leading to fewer target cells in the area of infection and thus to slower viral spread.

such that during the time frame of the simulation a hollow ring has not yet formed and the infected cell population expands as a relatively solid mass. In Figure 4b, the death probability of infected cells is higher such that during the time frame of the simulation a hollow ring has formed. The total number of cells is proportional to $\frac{e^{-At}-1+At}{A^2}$ [42], such that for short time-scales (or smaller death rates) the growth is quadratic in time, and for longer times scales (or larger death rates) it is linear in time. This is exactly what is observed. Figure 4a, characterized by smaller values of A, shows a growth law of the infected cell population that is close to quadratic. In Figure 4b, where the death rate is larger, the infected cell population grows linearly once the hollow ring is present. Note that these two scenarios are identical in principle because in Figure 4a, the formation of the hollow ring requires more time (and a larger grid). The higher the death rate of infected cells, the faster the ring is formed, and the faster the growth law changes from square to linear. Lowering the rate of virus spread (decreasing the value of B and increasing the value of A) gives rise to patterns of a different nature.

In Figure 4c, uninfected cells are left behind in the core of the expanding ring. When they grow and become infected by virus, a coupled expanding ring of uninfected and infected cells forms. This can occur repeatedly, giving rise to concentric rings. The persistence of cells in the core of the ring is probabilistic in nature, and that is reflected in the growth laws that are observed in multiple runs of the simulation. In cases where uninfected cells are not left behind inside the ring, the infected cell population grows linearly. When concentric rings do occur, the growth becomes quadratic.

Finally, no expanding ring structure is formed in Figure 4d because the viral spread kinetics are even slower. Instead, the area of virus growth is characterized by a mix of infected and uninfected cells that expands over time. In this case, quadratic growth of infected cells is observed. Note that if the viral spread kinetics are in the lower end of this spectrum, it is possible to observe a variation of this pattern, shown in the inset of Figure 4d: While the spreading infection leaves uninfected cells behind, the viral spread kinetics are too low to maintain significant numbers of infected cells throughout this area. Most of the infected cells will be at the outer edge of the infection due to a higher density of target cells. In this case, a relatively thin, ring-like structure can be formed, with a large area of uninfected cells remaining in its core. This pattern, however, is temporary. With time, one of two scenarios can be observed. A mixed pattern can be generated, characterized by a large number of uninfected cells and a low number of infected cells, because the virus eventually spreads to the remaining susceptible cells. Alternatively, there is a chance that the virus population goes extinct due to the slow rate of spread. Long term outcomes are discussed further below.

4.2. **Growth patterns and the extinction of cells.** Here, we explore the long term dynamics, investigating how the above described patterns play out and correlate with the overall outcome if both the uninfected and infected cell population can expand in space. We seek to define conditions under which the virus can eliminate the target cell population in this system. All simulations are started with a small number of infected cells placed in a compact vicinity into a larger space filled with uninfected cells, which is in turn embedded into an even larger "empty" space (for the exact initial conditions for particular cases, see appropriate figure legends). In contrast to the simulations reported above, here we go beyond the initial virus

growth stage, and focus on time-scales where the population of target cells experiences significant changes (grows in size in the absence of infection). The outcomes of this system include extinction of the target cells and thus the virus; extinction of the virus and persistence of the target cells; coexistence of virus and target cells. The dependency of these outcomes on the parameters is shown in Figure 5, which

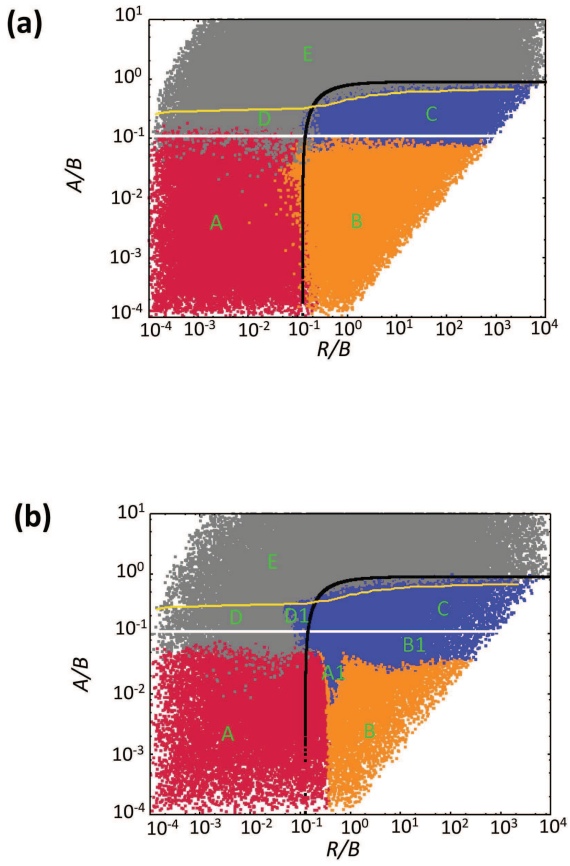

FIGURE 5. Dependence of outcomes on parameters in the agent-based model for (a) a 30×30 grid, and (b) a 300×300 grid. Blue means coexistence of virus and cells. Red and orange indicate extinction of the cells and thus the virus. Red is used if extinction occurs before the boundary of the system has been reached, while orange is used if extinction occurs after cells have reached the boundary of the system. Grey indicates extinction of the virus while cells persist. Above the white line and below the black line, the "local" equilibrium number of uninfected and infected cells, respectively, is greater than one. Below the yellow line, the virus can successfully invade its target cell population. The capital letters indicate different spatial patterns that are described in the text and in figure 6. In these simulations, the probability for an uninfected cell to die was D=0.

is the result of at least 10^4 instances of the simulation, where the $\log_{10}$ of all the parameters was varied between -4 and 4. Figures 6 and 7 show corresponding spatial and temporal patterns. We examine the outcomes first in a relatively small *30x30* grid, and subsequently in a larger, *300x300* grid.

Small grid. In the 30x30 grid, the following outcomes are found (Figure 5a, and Figures 6 & 7).

Two types of target cell extinction can be observed, both associated with the initial "hollow ring" structure. According to pattern **A**, ***virus-mediated target cell extinction***, both the target cell and the virus populations spread outward in space as a wave, but the virus wave overtakes the target cell wave, leading to extinction of both populations. Pattern **B**, ***boundary-mediated extinction***, represents weaker viruses compared to case A. In pattern B, the virus wave catches up with the target cell wave, leaves no uninfected cells behind in its wake, but fails to eliminate the target cell wave. Instead, the two waves travel together with the

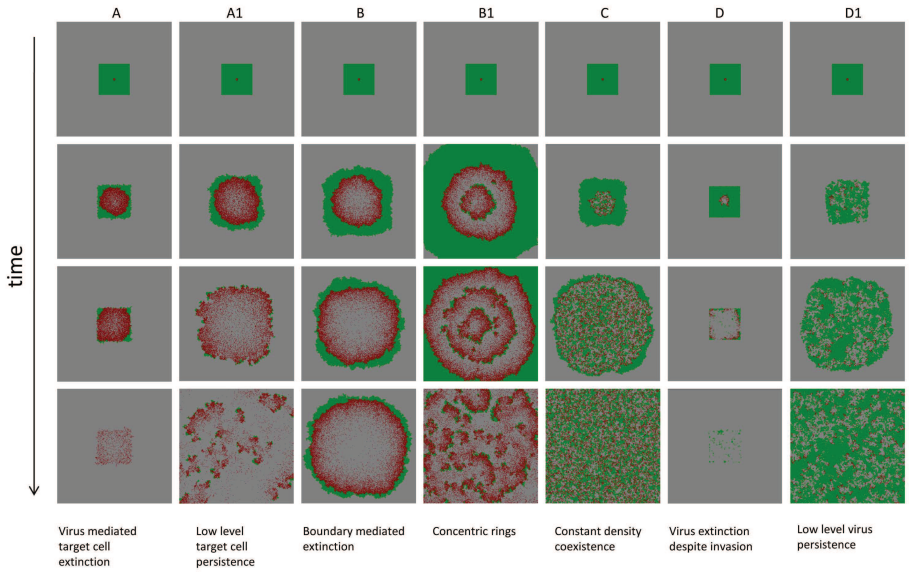

FIGURE 6. Seven spatial patterns observed in the agent-based model. For each pattern, four snapshots in time are shown. Green indicates uninfected cells, red infected cells, and grey empty patches. See corresponding capital letters in figure 5, showing in which parameter regions the individual patterns are observed. The time series that are associated with the individual patterns are shown in figure 7. See text for details. The simulations were run on a 300×300 grid. The simulations were started by placing a small number of infected cells (5×5 cells) into a larger space filled with infected cells (13×13 cells). Parameters were chosen as follows: (A) R=0.013; D=0; B=0.14; A=0.003; (A1) R=0.15; D=0; B=0.32; A=0.007; (B) R=0.014; D=0; B=0.015; A=0.00056; (B1) R=0.04; D=0; B=0.032; A=0.0016; (C) R= 0.014; D=0; B=0.032; A=0.008; (D) R=0.0002; D=0; B=0.019; A=0.0032; (D1) R=0.069; D=0; B=0.64; A=0.18.

same velocity until the boundary in reached. The target cell population can escape the virus only by spreading outward. Once the boundary is reached, this is not possible anymore, explaining the extinction. Note that although real tumors are capable of breaking out of homeostatic control and spreading beyond the "carrying capacity" of their environment, boundary-mediated extinction can still take place. Genetic transformations associated with waves of clonal expansion or induction angiogenesis generally happen on longer time-scales. Therefore, it is realistic to assume the existence of some geometric constraints (even temporary). Pattern B represents the situation where extinction is a consequence of such spatial constraints.

Another type of outcome is the coexistence of infected and uninfected cells, which is shown in pattern **C**, ***constant density coexistence***. As the virus population spreads out in space, it leaves behind uninfected cells with a high probability, leading to the disperse pattern of initial expansion and the absence of any clear traveling waves. Instead, the expanding virus population leaves behind a mix of both populations, which eventually is found across the whole space and is characterized by an equilibrium density that is determined by the parameters of the system, while the populations settle around a stochastic steady state.

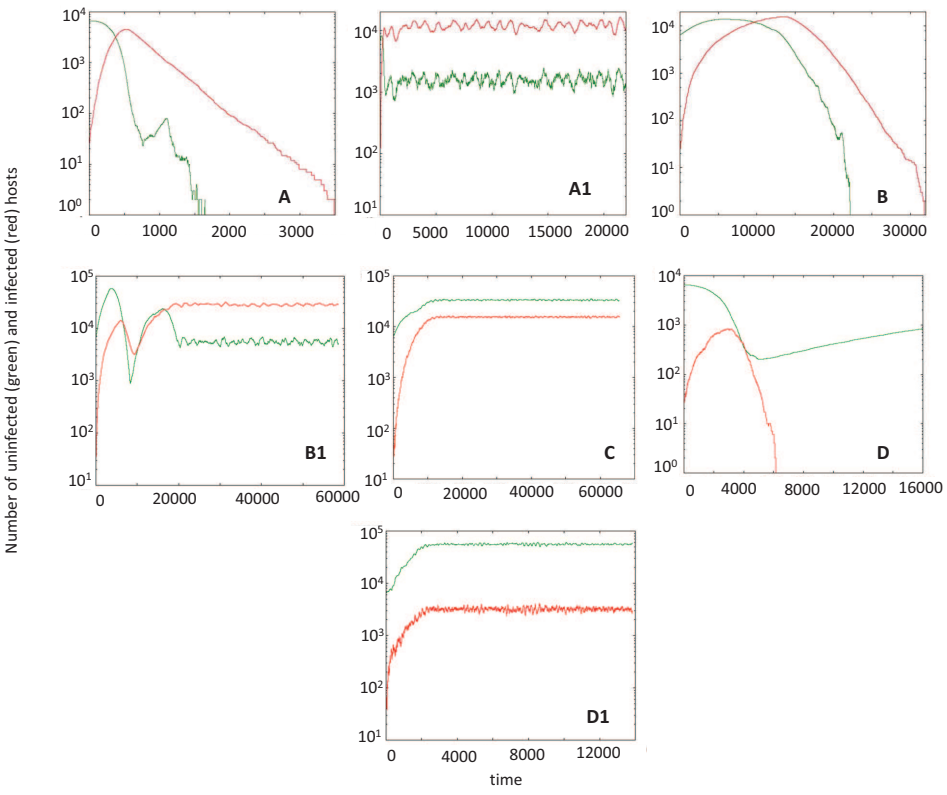

FIGURE 7. Typical time series corresponding to the spatial patterns presented in figure 6, based on a single run of the spatial agent based model, assuming a *300x300* grid. See text for details. Parameter values and initial conditions are given in figure 6.

Finally, there are two types of virus extinction patterns. Pattern **D**, ***virus extinction despite invasion***, represents a virus extinction regime where the virus can initially invade the target cell population, but does not persist in the long term. The virus reduces the target cell population, and subsequently goes extinct. This leaves the uninfected cell population to grow unopposed. The stronger the virus (lower value of A/B), the less likely this is observed in this regime, because the uninfected cell population is more likely to be driven extinct before the virus population hits extinction. The second extinction pattern **E**, ***lack of invasion***, is observed when the virus population cannot invade the target cell population and goes extinct (spatial and temporal pattern not shown).

Although the spatial stochastic predator-prey system studied here exhibits a variety of patterns, its dynamics can be understood by studying the local interactions of the agents. The idea of a "characteristic scale" has been proposed in the literature in the context of different predator-prey models [44] where the system's behavior was found most predictable on an intermediate scale defined by the agents' motility and interactions. In [45], it was shown that in a class of systems exhibiting oscillatory dynamics, the functional forms governing the local predator-prey interactions at those characteristic scales are the same as the ones describing a perfectly mixed, mass-action system, but contain different parameters. This allowed the authors to approximate the long-term dynamics of the spatial system at large scales with a temporal predator-prey model describing local interactions. In this paper we will build on this idea, and show that the global outcomes of the spatially-distributed system can be predicted by utilizing the laws of local dynamics.

We start from the well-known system of ordinary differential equations that can be derived for our agent-based model if no spatial restrictions were in place, and reproduction and infection events were driven by laws of mass-action:

$$\begin{aligned} \frac{dS}{dt} &= RS\left(1-\frac{S+I}{K}\right)-\frac{BSI}{K}, \\ \frac{dI}{dt} &= \frac{BSI}{K}-AI, \end{aligned} \tag{2}$$

where the number of uninfected cells is denoted by S, and the number of infected cells by I. In these equations, K has the meaning of carrying capacity. This well-known modified Lotka-Volterra system [46, 47] is characterized by two equilibria: (i) The uninfected population persists at carrying capacity, while the virus population is extinct, i.e. $S^{(0)} = K$, $I^{(0)} = 0$; (ii) Alternatively, the virus establishes a successful infection, such that $S^{(1)} = AK/\mathrm{B}, I^{(1)} = RK(\mathrm{B}-A)/\mathrm{B}(R+\mathrm{B})$. The latter equilibrium is stable if the basic reproductive ratio of the virus is greater than one, which is equivalent to the inequality A<B. The approach to the coexistence equilibrium can be either monotonic, or can involve damped oscillations.

While these properties of the virus-cell system are well-known, it is usually thought that the ordinary differential equations can only be applied to a well-mixed system, and fail to describe a spatially-distributed system of cells. Contrary to this, Figure 5 demonstrates that, if interpreted correctly, the above system can explain a lot of the patterns that arise in the spatial agent-based model. Let us think of the carrying capacity coefficient, K, as the size of the "local neighborhood" where cell-to-cell interactions happen in a spatial model. In our case, this neighborhood

consists of K=9 cells (a cell plus its eight nearest neighbors, the relevant characteristic scale of our spatial model). Model (2) with the modified parameter K are capable of informing us of the local equilibrium density of the infected and uninfected cells, which in term is correlated with the expected long term behavior of the spatial system.

In equations (2), the number of uninfected cells at the equilibrium (the value $S^{(1)}$) is proportional to K. In order for this equilibrium to be biologically meaningful, this value must be greater than one cell. The equation $S^{(1)} = 1$ defines the white line in Figure 5. Similarly, the number of infected cells in local neighborhoods must be greater than one, which yields the black line, $I^{(1)} = 1$. We can see that the coexistence region in Figure 5a (regime C) corresponds to the parameters for which both equilibrium values are larger than one; it is enclosed by the lines $S^{(1)} = 1$ and, $I^{(1)} = 1$ obtained directly from the cancer-virus equations. The white line $S^{(1)} = 1$ outlines the lower boundary of the coexistence region, while the black line $I^{(1)} = 1$ defines the upper boundary. (A more precise definition of the upper bound of the coexistence region is given by the yellow line in Figure 5a, below which the virus is strong enough to invade the cell population).

Thus, in the spatial system, target cell extinction is observed if the local equilibrium number of uninfected cells is less than one (regions A & B, Figure 5a, below white line). Extinction of virus only is observed either following initial invasion if its local equilibrium is less than one (region D, Figure 5a, area encased by white, black and yellow lines) or if invasion is impossible (region E, Figure 5a, above yellow line). The finding that equilibrium properties of simple ODE models that describe the dynamics in a small local neighborhood can predict the outcome of the spatial system has important practical implications. Note however that this method is unable to explain all the details of the diagram in Figure 5. In particular, the proximity of the black ($I^{(1)} = 1$) line to the boundary between regions A and B is purely coincidental. The equilibrium analysis predicts extinction in regions A and B, but cannot distinguish between virus-mediated extinction (A) and boundary-mediated extinction.

Large grid. In a larger, 300x300, grid (Figure 5b, and Figures 6 & 7), the basic patterns found in a small grid are still in place, but additional complexity is observed. In the parameter space where target cell extinction happens in the smaller grid, regions of coexistence can occur. In pattern **A1**, the expanding virus wave proceeds initially as a "hollow ring" structure, catches up with the target cell wave, leaves no uninfected cells in its wake, but only partially breaks the target cell wave. The virus is not efficient enough to eliminate the target cell wave, as observed in pattern A, but still strong enough not to leave it intact, as observed in pattern B. The partially broken wave structure allows the uninfected cells to escape not only outward, but in all directions. Hence, local extinction combined with continuous target cell movement away from the virus leads to persisting moving fronts, which can go extinct and give rise to new fronts over time. Thus, more extensive population fluctuations are observed in the long run (Figure 7). This is the well-known regime of global persistence despite local extinction which is an important basis for the argument that space promotes coexistence [48]. The levels at which the uninfected cell population persists, however, are relatively low (Figure 7). A sufficiently large grid size is required to observe this behavior, such that enough space is available for the moving target cell fronts to persist. We refer to pattern A1 as ***low-level target cell persistence***. Region **B1** shows a different reason for target cell

persistence at low levels, a pattern we call ***concentric rings***, which corresponds to the concentric ring pattern of initial virus spread described earlier. When the virus wave expands, the probability to leave behind uninfected cells is proportional to the local equilibrium number of uninfected cells. In the region where this equilibrium number is just slightly below one, this does not occur often enough to be observed on a small grid. On a larger grid, however, it can be observed. These infrequent events lead to renewed target cell growth, followed by virus growth, and a new wave structure is formed. This can lead to the occurrence of concentric expanding rings. With time, stochasticity breaks the ring structure, leading to traveling fronts that eventually go extinct, but occasionally leave behind uninfected cells to form new fronts, thus persisting in the long term. Consequently, populations show more extensive fluctuations around characteristic steady state values (Figure 7). For lower values of A/B, the local equilibrium number of uninfected cells becomes too low for this to be observed in the grid size under consideration. Finally, in region **D1**, ***low-level virus persistence***, global persistence of the virus despite local extinction is observed, leading to relatively strong population fluctuations (Figure 7). While the virus invades the target cell population, it converges to its local equilibrium value that is less than one. However, movement through space before extinction occurs allows coexistence if the grid is sufficiently large. For lower values of R/B, the local equilibrium number of infected cells is too low to observe this outcome even in the context of the larger grid.

These simulations show that increasing the grid size allows more complex outcomes to occur and increases the parameter region in which the cell populations persist. The additional patterns that emerge in larger grids are variations of those found in the smaller grid and involve non-equilibrium persistence, where extinction occurs locally, but movement through space allows cells to temporarily avoid extinction. These dynamics are well documented in the ecological literature [48]. Besides allowing cells to move through space, a larger grid size also increases the chances that certain rare events can occur. For example, boundary-mediated extinction (pattern B, Figure 5) is less likely to occur in large grids. The larger the grid the higher the probability that uninfected cells are left in the core of the ring before the uninfected cell population has moved to the boundary and is eliminated by the virus. All these non-equilibrium persistence outcomes in larger grids, however, are characterized by persistence of the cells at very low levels, which can be considered controlled persistence and does not involve uncontrolled cellular growth. Therefore, the outcome can still be predicted by the "local mass action equilibrium values" discussed above: if the local equilibrium of uninfected cells, predicted by the ODEs, is less than one, we can expect either extinction or controlled persistence. If the local equilibrium of uninfected cells is greater than one, we can expect to see uncontrolled cellular growth. The lower the local equilibrium of uninfected cells the less likely controlled persistence occurs and the more likely extinction is observed. However, this could not be demonstrated systematically for larger grids due to the extensive computational costs involved.

The long term outcomes shown in Figure 6 are obviously related to the initial growth patterns described in Figure 4. Patterns A, A1 and B in Figure 6 arise out of the hollow-ring structure. Pattern B1 in Figure 6 emerges from the concentric ring structure. Patterns C, D, and D1 are consequences of the disperse growth pattern / filled ring structure, which for faster viral spread rates typically leads to coexistence

of the virus and cell populations, while extinction of the virus population can be observed for smaller virus spread rates.

5. **Conclusions.** This review summarized various modeling approaches that we have employed to study the dynamics of oncolytic viruses. Ordinary differential equations have been heavily employed in the field of virus dynamics in general, and have given rise to many biologically useful results [47]. The same applies to oncolytic virus dynamics, especially with respect to some very fundamental concepts and predictions. At the same time, this modeling approach has weaknesses that limit the predictive power of such models in more advanced settings where precise treatment regimes need to be worked out in the context of specific viruses and cancers. One of the problems with the ODE approach is that equations contain arbitrary mathematical expressions that could be equally well described by alternative terms that change the properties of the model. In most cases, the "biologically correct" formulation is not known. Thus, a general, axiomatic modeling approach can be useful, where analysis does not focus on specific models, but on classes of models characterized by biological constraints. Another important limitation of the ODE approach is that spatial aspects of tumors cannot be accounted for explicitly. To do so, alternative modeling techniques need to be utilized, and we have described a spatially explicit agent-based model in this respect. In all modeling approaches, it is important to realize that the biological complexity of the system is enormous and largely not well understood, which again limits the predictive power of models. A reasonable strategy described here is to first focus on relatively simple settings, such as in vitro systems, in which most assumptions are relatively well understood. This allows the model to be tested and validated by specific experiments [42]. Once the simplest setting can be described adequately with a model, additional biological complexities can be incorporated one step at a time. The ultimate goal of this work is to generate a biologically realistic model for the treatment of tumors in vivo, which has solid predictive power and can be used to optimize treatment strategies.

REFERENCES

[1] J. C. Bell, *Oncolytic viruses: What's next?*, Curr. Cancer Drug Targets, **7** (2007), 127–131.

[2] J. C. Bell, B. Lichty and D. Stojdl, *Getting oncolytic virus therapies off the ground*, Cancer Cell, **4** (2003), 7–11.

[3] A. M. Crompton and D. H. Kirn, *From ONYX-015 to armed vaccinia viruses: The education and evolution of oncolytic virus development*, Curr. Cancer Drug Targets, **7** (2007), 133–139.

[4] J. J. Davis and B. Fang, *Oncolytic virotherapy for cancer treatment: Challenges and solutions*, J. Gene. Med., **7** (2005), 1380–1389.

[5] J. M. Kaplan, *Adenovirus-based cancer gene therapy*, Curr. Gene Ther., **5** (2005), 595–605.

[6] E. Kelly and S. J. Russell, *History of oncolytic viruses: Genesis to genetic engineering*, Mol. Ther., **15** (2007), 651–659.

[7] D. H. Kirn and F. McCormick, *Replicating viruses as selective cancer therapeutics*, Mol. Med. Today, **2** (1996), 519–527.

[8] F. McCormick, *Cancer-specific viruses and the development of ONYX-015*, Cancer Biol. Ther., **2** (2003), S157–60.

[9] F. McCormick, *Future prospects for oncolytic therapy*, Oncogene, **24** (2005), 7817–7819.

[10] C. C. O'Shea, *Viruses - seeking and destroying the tumor program*, Oncogene, **24** (2005), 7640–7655.

[11] K. A. Parato, et. al., *Recent progress in the battle between oncolytic viruses and tumours*, Nat. Rev. Cancer, **5** (2005), 965–976.

[12] D. E. Post, et. al., *Cancer scene investigation: how a cold virus became a tumor killer*, Future Oncol., **1** (2005), 247–258.

[13] M. S. Roberts, et. al., *Naturally oncolytic viruses*, Curr. Opin. Mol. Ther., **8** (2006), 314–321.

[14] M. J. Vaha-Koskela, J. E. Heikkila and A. E. Hinkkanen, *Oncolytic viruses in cancer therapy*, Cancer Lett., (2007).

[15] H. H. Wong, N. R. Lemoine and Y. Wang, *Oncolytic viruses for cancer therapy: Overcoming the obstacles*, Viruses, **2** (2010), 78–106.

[16] D. Koppers-Lalic and R. C. Hoeben, *Non-human viruses developed as therapeutic agent for use in humans*, Rev. Med. Virol, **21** (2011), 227–239.

[17] R. L. Martuza, et. al., *Experimental therapy of human glioma by means of a genetically engineered virus mutant*, Science, **252** (1991), 854–856.

[18] K. Garber, *China approves world's first oncolytic virus therapy for cancer treatment*, J. Natl. Cancer Inst., **98** (2006), 298–300.

[19] R. M. Eager and J. Nemunaitis, *Clinical development directions in oncolytic viral therapy*, Cancer Gene. Ther., **18** (2011), 305–317.

[20] D. Wodarz, *Viruses as antitumor weapons: Defining conditions for tumor remission*, Cancer Res., **61** (2001), 3501–3507.

[21] D. Wodarz, *Gene therapy for killing p53-negative cancer cells: Use of replicating versus nonreplicating agents*, Hum. Gene. Ther., **14** (2003), 153–159.

[22] Z. Bajzer, et. al., *Modeling of cancer virotherapy with recombinant measles viruses*, J. Theor. Biol., **252** (2008), 109–122.

[23] M. Biesecker, et. al., *Optimization of virotherapy for cancer*, Bull. Math. Biol., **72** (2010), 469–489.

[24] D. Dingli, et. al., *Mathematical modeling of cancer radiovirotherapy*, Math. Biosci., **199** (2006), 55–78.

[25] D. Dingli, et. al., *Dynamics of multiple myeloma tumor therapy with a recombinant measles virus*, Cancer Gene Ther., **16** (2009), 873–882.

[26] A. Friedman, et. al., *Glioma virotherapy: Effects of innate immune suppression and increased viral replication capacity*, Cancer Res., **66** (2006), 2314–2319.

[27] G. P. Karev, A. S. Novozhilov and E. V. Koonin, *Mathematical modeling of tumor therapy with oncolytic viruses: effects of parametric heterogeneity on cell dynamics*, Biol. Direct, **1** (2006), pp. 30.

[28] N. L. Komarova and D. Wodarz, *ODE models for oncolytic virus dynamics*, J. Theor. Biol., **263** (2010), 530–543.

[29] A. S. Novozhilov, et. al., *Mathematical modeling of tumor therapy with oncolytic viruses: Regimes with complete tumor elimination within the framework of deterministic models*, Biol. Direct, **1** (2006), pp. 6.

[30] L. M. Wein, J. T. Wu and D. H. Kirn, *Validation and analysis of a mathematical model of a replication-competent oncolytic virus for cancer treatment: Implications for virus design and delivery*, Cancer Res., **63** (2003), 1317–1324.

[31] D. Wodarz, *Computational approaches to study oncolytic virus therapy: Insights and challenges*, Gene Therapy and Molecular Biology, **8** (2004), 137–146.

[32] D. Wodarz, *Use of oncolytic viruses for the eradication of drug-resistant cancer cells*, J. R. Soc. Interface, **6** (2009), 179–186.

[33] D. Wodarz and N. Komarova, *Towards predictive computational models of oncolytic virus therapy: Basis for experimental validation and model selection*, PLoS ONE, **4** (2009), e4271.

[34] N. Bagheri, et. al., *A dynamical systems model for combinatorial cancer therapy enhances oncolytic adenovirus efficacy by MEK-inhibition*, PLoS Comput. Biol., **7** (2011), e1001085.

[35] R. Zurakowski and D. Wodarz, *Model-driven approaches for in vitro combination therapy using ONYX-015 replicating oncolytic adenovirus*, J. Theor. Biol., **245** (2007), 1–8.

[36] W. Mok, et. al., *Mathematical modeling of herpes simplex virus distribution in solid tumors: Implications for cancer gene therapy*, Clin. Cancer Res., **15** (2009), 2352–2360.

[37] L. R. Paiva, et. al., *A multiscale mathematical model for oncolytic virotherapy*, Cancer Res., **69** (2009), 1205–1211.

[38] C. L. Reis, et. al., *In silico evolutionary dynamics of tumour virotherapy*, Integr. Biol. (Camb), **2** (2010), 41–45.

[39] L. You, C. T. Yang and D. M. Jablons, *ONYX-015 works synergistically with chemotherapy in lung cancer cell lines and primary cultures freshly made from lung cancer patients*, Cancer Res., **60** (2000), 1009–1013.

[40] A. Chahlavi, et. al., *Replication-competent herpes simplex virus vector G207 and cisplatin combination therapy for head and neck squamous cell carcinoma*, Neoplasia, **1** (1999), 162–169.

[41] I. A. Rodriguez-Brenes, N. L. Komarova and D. Wodarz, *Evolutionary dynamics of feedback escape and the development of stem-cell-driven cancers*, Proc. Natl. Acad. Sci. U S A, **108** (2011), 18983–18988.

[42] D. Wodarz, et. al., *Complex spatial dynamics of oncolytic viruses in vitro: Mathematical and experimental approaches*, PLoS Comput. Biol., **8** (2012), e1002547.

[43] K. Sato, H. Matsuda and A. Sasaki, *Pathogen invasion and host extinction in lattice structured populations*, Journal of Mathematical Biology, **32** (1994), 251–268.

[44] A. M. Deroos, E. Mccauley and W. G. Wilson, *Mobility versus density-limited predator prey dynamics on different spatial scales*, Proceedings of the Royal Society of London Series B-Biological Sciences, **246** (1991), 117–122.

[45] M. Pascual, P. Mazzega and S. A. Levin, *Oscillatory dynamics and spatial scale: The role of noise and unresolved pattern*, Ecology, **82** (2001), 2357–2369.

[46] R. M. Anderson and R. M. May, "Infectious Diseases of Humans," 1991, Oxford, England: Oxford University Press.

[47] M. A. Nowak and R. M. May, "Virus Dynamics. Mathematical Principles of Immunology and Virology," 2000: Oxford University Press.

[48] M. P. Hassell, "The Spatial and Temporal Dynamics of Host-Parasitoid Interactions," 2000, Oxford: Oxford University Press.

Received July 20, 2012; Accepted February 01, 2013.

E-mail address: dwodarz@uci.edu